Photonics and Nanostructures - Fundamentals and Applications 61 (2024) 101295

Contents lists available at ScienceDirect

Photonics and Nanostructures - Fundamentals and Applications

journal homepage: www.elsevier.com/locate/photonics

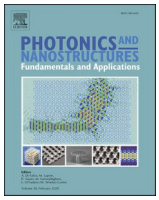

Frequency tunable mid-infrared split ring resonators on a phase change material

Laurent Boulley, Paul Goulain, Pierre Laffaille, Thomas Maroutian, Raffaele Colombelli, Adel Bousseksou *

Centre de Nanosciences et Nanotechnologies, Université Paris-Saclay, CNRS, UMR 9001, 91120 Palaiseau, France

ARTICLE INFO

Keywords:
Optoelectronics
Meta-surfaces
Split-ring resonators (SRR)
Phase change material
Vanadium dioxide VO_2
Pulsed laser ablation
Tunability

ABSTRACT

Meta-surfaces arrays are 2D meta-materials with a periodicity below the diffraction limit that permits to obtain homogeneous layers of resonant effective refractive index. In this work we present an analytical model that describes the electromagnetic behavior of meta-surfaces constituted by split-ring resonators (SRR). SRR resonance frequency can be adjusted by choosing their geometric parameters and the materials they are made of. Their deposition on a phase change material enables an optical modulation of resonance peak during the phase transition. We demonstrate a mid-infrared tunable SRR meta-surface using Vanadium dioxide (VO_2) as phase change material deposited on III-V semiconductors by low temperature pulsed laser ablation technique. The presented measurements exhibit a maximum of 100 cm^{-1} resonance shift. This result is very promising for the conception of monolithic, robust, compact, frequency tunable III-V based devices in the mid-infrared.

Abstract

Meta-materials (MM) are resonant artificial and technically controlled materials whose properties reproduce and go beyond the electronic atomic resonance. Consequently called “meta-atoms”, their dielectric permittivity, magnetic permeability, refractive index and optical absorption can be chosen according to their geometric parameters and the materials they are made of. MM are electromagnetic filters, ie. compact, passive and low energy consuming frequency selective surfaces allowing to obtain a specific electromagnetic response. They are principally used in the microwave domain [32,40], in transformation optics, invisibility cloaking [26], sub wavelength imaging, index gradient materials, negative refractive indexes [34–36], super-lenses [25] and perfect absorbers [12].

Meta-materials arrays are below the diffraction limit, meaning that the layer composed by the nanoscopic resonators array is no more diffractive but can be considered as a macroscopic homogeneous layer modeled as a composite with effective permittivity, permeability and refractive optical index. The diffraction limit comes from the Heisenberg uncertainty principle in quantum mechanics stipulating that if two observables do not commute, then it is not possible to know exactly and simultaneously both values of them. In the case of the conjugated observables position x and momentum p_x, the uncertainty relation for the standard deviation in position Δx and in momentum Δp_x writes [8]:

$$\Delta x \Delta p_x \geq \hbar/2 \tag{1}$$

where $\hbar$ is the reduced Planck constant, meaning that it is not possible to know the position and the momentum of a particle at the same time. This is the corpuscle point of view. Reformulating it with the De Broglie relation:

$$p_x = \hbar k_x \tag{2}$$

where k_x is the wave vector along the x axis, we obtain the wave-like point of view:

$$\Delta x \Delta k_x \geq 1/2 \tag{3}$$

where Δk_x is the standard deviation in wavevector, meaning that a monochromatic wave is spatially delocalized whereas it becomes a wave packet with a spectral enlargement. As there is the same uncertainty relation along the y coordinate, we also have:

$$\Delta y \Delta k_y \geq 1/2 \tag{4}$$

In the case of a diffracting opening, a condition on the position of the plane wave or the wave packet and the particle is imposed, and the wave vector remains undetermined. In order to determine the diffraction

* Corresponding author.
E-mail address: adel.bousseksou@c2n.upsaclay.fr (A. Bousseksou).

https://doi.org/10.1016/j.photonics.2024.101295
Received 2 October 2023; Received in revised form 14 June 2024; Accepted 28 June 2024
Available online 5 July 2024

limit, both uncertainties on the position and on the wavevector need to be minimized. The minimum standard deviation for the wave vector Δk corresponds to the uncertainty on the number of states k down to dk in the reciprocal space: it is the density of states in wave vector by surface unit.

If one consider a particle confined in a plane in a square of length L and of surface $A = L^2$, the resolution of the stationary Schrödinger equation with null edge conditions implies that each wavevector state of the particle occupies a surface $\left(\frac{\pi}{L}\right)^2 = \frac{\pi^2}{A}$ in the reciprocal space as schematized in Fig. 1. The circular ring surface defined by wavevector states of norm k down to dk, ie. the surface defined between the circles of radius k and $k+dk$, has a surface equal to $2\pi k dk$. The number of states dn_k of wavevector k down to dk is defined as the number of surfaces $\frac{\pi^2}{A}$ comprised in a quarter of the circular ring surface, corresponding to the positive values of the wavevector. Taking the degeneration into account, we obtain:

$$dn_k = 2\frac{2\pi k dk}{4}\frac{1}{\frac{\pi^2}{A}} = \frac{k}{\pi}dkA \tag{5}$$

The density of states in wave vector by surface unit is defined as:

$$\Delta k = \frac{1}{A}\frac{dn_k}{dk} \tag{6}$$

From Eqs. (5) and (6), we conclude:

$$\Delta k = \frac{k}{\pi} \tag{7}$$

From the Euclidian norm, we have

$$\Delta r = \left[(\Delta x)^2 + (\Delta y)^2\right]^{1/2} \text{and} \Delta k = \left[(\Delta k_x)^2 + (\Delta k_y)^2\right]^{1/2}$$

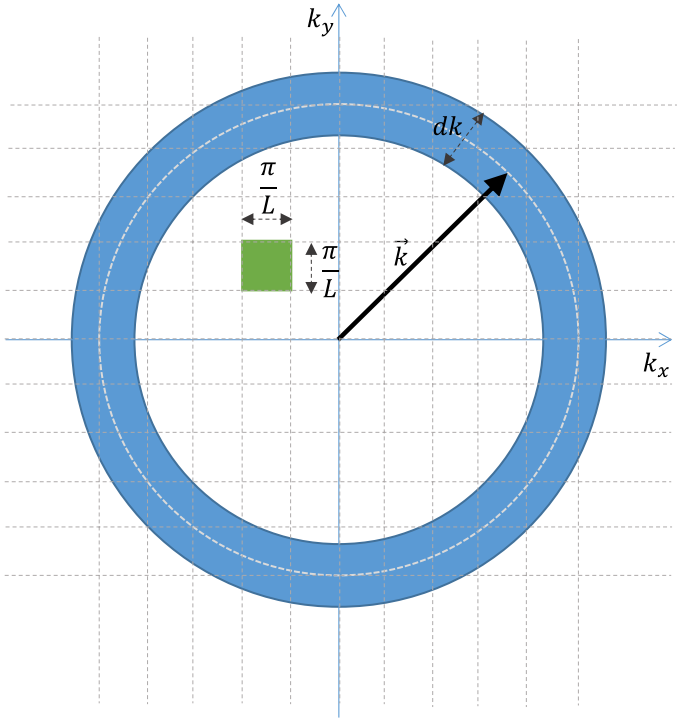

Fig. 1. Schematics of the surface occupied by each wavevector state in the reciprocal space (green square) for a particle confined in a plane in a square of length L and of the surface of the circular ring defined by wavevector states of norm k down to dk, ie. the surface defined between the circles of radius k and $k+dk$ (blue ring) used to compute the number of states dn_k of wavevector k down to dk and deduce the density of states in wavevector by surface unit Δk.

and combining with Eqs. (3) and (4), we have:

$$\Delta r \Delta k \geq 1 \tag{8}$$

According to Eqs. (7) and (8), the inferior limit for the uncertainty on the position is deduced:

$$\Delta r = \frac{\lambda_0}{2n} \tag{9}$$

with λ_0 the vacuum wavelength and n the medium optical refractive index.

Eq. (9) gives the optical formulation of the Heisenberg principle: this is the optical diffraction limit. It is coherent with the Abbe diffraction limit for an optical system and with the electromagnetic field confinement limit in a cavity, eg. it is the minimum length cavity in a Fabry-Perot resonator and it is the grating periodicity in a first order distributed feedback network where λ_0 is then the Bragg wavelength. In choosing an uncertainty on the position smaller than the diffraction limit, uncertainty on the wave vector increases and the diffractive character of the optical system is lost. Thus the structuration of the MM array with a sub wavelength periodicity forms a macroscopic homogeneous layer, which properties only depend on geometrical parameters of the nanoscopic MM elements.

Analogy between electronics and electromagnetics makes easier the modeling and the control of the interaction of MM with an electromagnetic field. The electrical values that are the current intensity I, the electrical potential V and the electrical bias U are linked with the electromagnetic values that are the electric polarization $\vec{P}$, the magnetic polarization $\vec{M}$, the electric field $\vec{E}$, the displacement vector $\vec{D}$, the magnetic field $\vec{B}$ and the magnetic excitation vector $\vec{H}$. Meta-surfaces are composed of metal, it is thus possible to consider them as electrical Resistor, Inductor and Capacitor (RLC) circuits in a series, which impedance Z, defined such as $U = ZI$, is for a plane wave $X = X_0 e^{i(\vec{k}.\vec{r}-\omega t)}$ in the quasi-stationary approximation:

$$Z = R - i\omega L - \frac{1}{i\omega C} \tag{10}$$

As RLC circuits in a series are second order filters, they can be resonant. For the electric resonance, as shown on Fig. 2.a, MM can be modeled by simply linear antennas of length l and of section S that can be considered as electric dipoles. Dipolar momentum $\vec{p} = q\vec{r}$ where q is the charge carried by each pole and $\vec{r}$ the distance between the poles gives rise to the polarization $\vec{P} = \frac{1}{\mathscr{V}}q\vec{r}$ that is the dipolar moment density with $\mathscr{V}$ the dipole volume. As the polarization current density writes: $\overrightarrow{j_{pol}} = \frac{1}{\mathscr{V}}q\vec{v}$ where $\vec{v}$ is the charge carries velocity and as $I = j_{pol}S$, we deduce in the sinusoidal regime:

$$I = -i\omega SP \tag{11}$$

Polarization $\vec{P}$ is also linked to the electric field $\vec{E}$ by the dielectric susceptibility χ_e: $\vec{P} = \varepsilon_0\chi_e \vec{E}$. As $\vec{E} = -\overrightarrow{grad}V$, we deduce $U = El$ where U is the electrical bias at the antenna boundaries resulting from the electrical potential difference at the two edges of the antenna.

Thus

$$P = \varepsilon_0\chi_e\frac{U}{\ell} \tag{12}$$

which combined to (11) leads to:

$$\chi_e = \frac{i}{\varepsilon_0\omega}\frac{\ell}{S}\frac{I}{U} = \frac{i}{\varepsilon_0\omega}\frac{\ell}{S}\frac{1}{Z} \tag{13}$$

Replacing Z with its expression (10), we get a Thomson-Lorentz like model, similar to the electronic atomic resonance [31]:

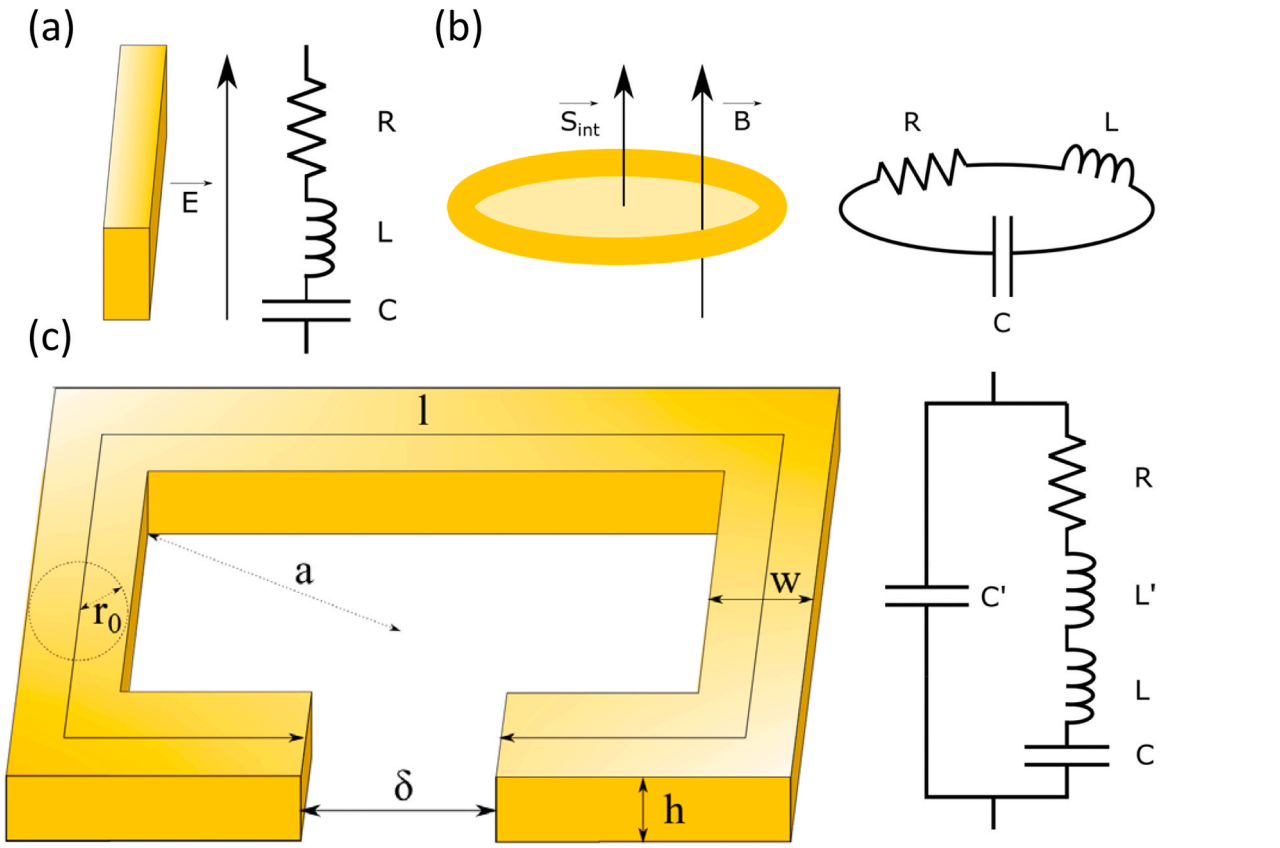

Fig. 2. (a) Schematic of the linear antenna and corresponding electrical RLC circuit. (b) Schematic of the loop antenna and corresponding RLC circuit. (c) Schematic of the Split Ring Resonator (SRR) and corresponding electrical RLC circuit. The SRR made of gold has a gap δ, a total length $\mathscr{l}$, a height h and a section S. In first approximation, the resonator can be taken similar to that of a tore with a the radius of the circular loop (tore) and r_0 the radius of its circular cross section.

$$\chi_e = \frac{-\frac{\mathscr{l}}{\varepsilon_0 SL}}{\omega^2 - \frac{1}{LC} + i\omega\frac{R}{L}} = \frac{-\omega_p^2}{\omega^2 - \omega_0^2 + i\Gamma\omega} \tag{14}$$

with $\omega_p^2 = \frac{1}{\varepsilon_0}\frac{\mathscr{l}}{S}\frac{1}{L}$ the plasma pulsation, $\omega_0 = \sqrt{\frac{1}{LC}}$ the eigen pulsation, similar to the electronic atomic resonance pulsation between two electronic levels and $\Gamma = \frac{R}{L}$ is the damping factor, similar to a fluid friction force in the atom classical model. Bandwidth is $\Delta\omega = \Gamma = \frac{R}{L}$ and quality factor is $Q = \frac{\omega_0}{\Delta\omega} = \frac{\omega_0}{\Gamma} = \frac{1}{R}\sqrt{\frac{L}{C}}$.

For the magnetic resonance, MM can be modeled by simply current loops of length l and of internal surface S_{int}, as on Fig. 2.b, that are considered as magnetic dipoles [14,22]. Magnetic dipolar momentum $\vec{m} = I\overrightarrow{S_{\text{int}}}$ where I is the current in the loop and $\overrightarrow{S_{\text{int}}}$ is the normal vector to the internal surface of norm S_{int} [15], gives rise to the magnetization

$$\vec{M} = \frac{1}{\mathscr{V}}\vec{m} = \frac{1}{\mathscr{V}}I\overrightarrow{S_{\text{int}}} \tag{15}$$

that is the magnetic dipolar moment density with $\mathscr{V}$ the dipole volume.

Considering a magnetic field $\vec{B}$ applied along the normal direction to the internal surface, the electromotive force U_{mag} created by the magnetic flux $\phi = BS_{\text{int}}$ is given by the Faraday's law: $U_{mag} = -\frac{d\Phi}{dt} = -S_{\text{int}}\frac{dB}{dt}$. As the current loop is made of a non-magnetic material, typically gold, its relative permeability is unity and in a sinusoidal regime, we deduce $\vec{B} = \mu_0\vec{H}$ and

$$U_{mag} = S_{\text{int}}i\omega B = \mu_0 S_{\text{int}}i\omega H \tag{16}$$

Magnetization $\vec{M}$ is also linked to the magnetic excitation $\vec{H}$ by the magnetic susceptibility χ_m: $\vec{M} = \chi_m \vec{H}$. With (16) it follows:

$$M = \chi_m\frac{U_{mag}}{\mu_0 S_{\text{int}}i\omega} \tag{17}$$

And combined with (15), we obtain:

$$\chi_m = \frac{1}{\mathscr{V}}\mu_0 S_{\text{int}}^2 i\omega\frac{I}{U_{mag}} = \frac{1}{\mathscr{V}}\mu_0 S_{\text{int}}^2 i\omega\frac{1}{Z} \tag{18}$$

Replacing Z with its expression (10), we get a Thomson-Lorentz like model:

$$\chi_m = \frac{-\frac{1}{\mathscr{V}}\mu_0 S_{\text{int}}^2\frac{1}{L}\omega^2}{\omega^2 - \frac{1}{LC} + i\omega\frac{R}{L}} = \frac{-F\omega^2}{\omega^2 - \omega_0^2 + i\Gamma\omega} \tag{19}$$

with the same notations as for the dielectric resonance and the inductive constant $F = \frac{1}{\mathscr{V}}\mu_0 S_{\text{int}}^2\frac{1}{L}$.

The effective optical index is directly driven by the magnetic and electric susceptibilities χ_m and χ_e as:

$$n_{eff}^2 = \varepsilon_r\mu_r = (\varepsilon_\infty + \chi_e)(\mu_\infty + \chi_m) \tag{20}$$

with ε_∞ and μ_∞ respectively the permittivity and the permeability for infinite pulsation. Thus, the refractive index can be made resonant as well as reflection, transmission and absorption that depend on the refractive index, enabling optical engineering through the choice of the geometrical parameters of the MM medium base element.

In our study, we focus on the electric LC resonance of the Split Ring Resonator (SRR) geometry [24]. SRR are considered as inclusions in the host matrix and as they are smaller than the diffraction limit, they constitute a homogeneous effective layer [5,22], which collective effects are taken into account through the Maxwell-Garnett approximation. Fig. 2.c depicts a typical SRR geometry. The LC electric resonance comes

from the gap δ introduced in the loop, in which the electric field becomes very intense in the direction perpendicular to the gap faces at the resonance frequency, as in a plane capacitor. The SRR geometry, similar to that of a tore, adds a supplemental geometric inductance $L' = \mu_0 a \ln\left(\frac{8a}{r_0}\right) = \mu_0 \frac{\ell}{4} \ln\left(\frac{8\ell}{w+h}\right)$, where $a \approx \frac{\ell}{4}$ is the radius of the circular loop (tore), $r_0 \approx \frac{h+w}{4}$ is the radius of its circular cross section, l is the total length, w is the width of the arms and h their height. The resulting resonance pulsation for the SRR is then: $\omega_r = \sqrt{\frac{1}{(L+L')C} - \frac{R^2}{2(L+L')^2}}$. In practice, $L' \gg L$ [14,16,17].

In our work we studied the tunability of the frequency resonances of a mid-infrared SRR based MM medium as function of the geometrical parameters (metallic gap δ, total length ℓ and section S). In order not to restrain to a frequency fixed by the resonators geometry but to add dynamic properties to MM, we also developed active control of these meta-structures using a phase change material VO_2 as a host substrate. In the microwave domain, tunability has been achieved using integrated RF electrical components [11]. Nevertheless, for higher frequencies such as terahertz (THz) or infrared (IR), other solutions are required. Consequently, new meta-materials have been developed. The seeked optoelectronic switching has always to be fast even ultra-fast in order to build performing switches and modulators. In most of cases, free carrier density of the substrate material or of the material included in the resonators openings is modified. This density is directly linked to the material conductivity and so to its electromagnetic and optical characteristics via its permittivity and its permeability. The change of the substrate physical characteristics [37] can be electrically [6,7,12], mechanically, thermally or optically [21,23,33] controlled and it tunes the resonance frequency of these MM structures, which are called hybrid materials. Other studies at other wavelength ranges use the phase change material VO_2 as the host substrate with different MM to achieve tunability in the near infrared [9] and in the far infrared [10]. Interests have also been shown for new phase change materials in the area of photonic in-memory computing but with the smallest possible resonant wavelength shift [28–30,41]. Noteworthy is the emerging technology using phase change materials for reconfigurable electrical-optical mixed devices in the visible and near infrared ([19,38]-2, [13]).

In our work we demonstrate a frequency tunable MM in the mid-infrared wavelength range on III-V semiconductors using a VO_2 low temperature deposition technique [3] compatible with active optoelectronic devices. VO_2 presents a metal/insulator transition (MIT) from an insulating phase at low temperature to a metallic phase at high temperature. The MIT is based on the carrier density variation and the band diagram modification through temperature [4,18,20,39]. Thus, the MIT changes the electric conductivity and therefore the permittivity, the refractive index and the optical reflectivity of the VO_2 layer [3]. The change of the host substrate refractive index affects directly the LC resonance of the SRR, where capacitance is defined as for a plane condenser between the two opposite faces of the antenna: $C = \varepsilon_0 \varepsilon_r \frac{S}{\delta}$ where ε_0 is the vacuum permittivity and ε_r is the relative permittivity of the host substrate.

Fig. 3 shows scanning electronic microscope images of the fabricated devices. The periodic array of SRR nano-resonators has been deposited on GaAs substrate and on VO_2 (150 nm thick) on GaAs substrate. The VO_2 layer has been deposited by Pulsed Laser Deposition [3]. The SRR array has been built with electron beam lithography (EBL), using PMMA A3 resist, 290 nm thickness. An evaporation of titanium (3 nm) and gold (80 nm) follows with a lift-off. Optical reflectivity characterizations of the samples have been carried out with an optical microscope coupled to a Fourier transform infrared (FTIR) spectrometer. The reflectivity spectra are divided by a reference spectrum obtained from a perfectly reflecting gold sample.

Fig. 4 presents the study of the frequency dependence on the geometrical parameters of the SRR. Fig. 4.a shows results on a GaAs substrate where the gap δ increases from 35 nm to 100 nm and where total length ℓ is fixed to 1960 nm and periodicity is fixed to 900 nm in both directions. Varying the gap opening means varying the geometric capacitor C in the electrical model. This induces a large variation of the SRR resonance frequency: the wider the gap, the higher the resonance frequency.

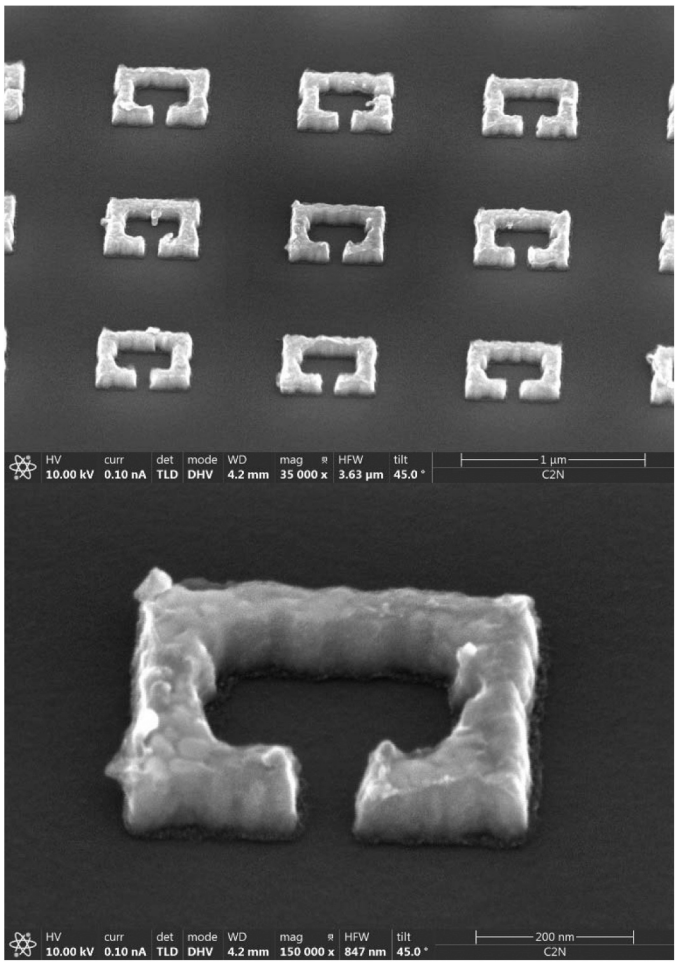

Fig. 3. Scanning Electron Microscope (SEM) images of a SRR array. SEM images measurements show a tolerance reproducibility of 2 nm on the SRR gap and a tolerance of 10–20 nm for the total length of the SRR.

Fig. 4.b shows the curves for SRR arrays on a VO_2 layer on a GaAs substrate. In this case, the total length varies from 1 µm to 2.05 µm and gap is fixed at 80 nm. Periodicity increases proportionally to the total length so that a constant density of resonators is kept in the arrays. The more the inductance, the less the resonance frequency and it has a lower influence on the resonance frequency variation. Indeed, the capacitor varies in 1/δ with δ the gap opening whereas the inductance has a logarithmic growth according to the effective length l. Besides, the measured quality factor of the SRR is around 10 leading to large resonance peaks. This value is not high because of the ohmic losses of the metal constituting the SRR antennas.

If we consider SRR of length l = 1.75 µm, of gap δ =80 nm with an height of h = 83 nm (orange SRR on Fig. 4.b), we obtain a resonant wavenumber of 1457 cm^{-1}, which corresponds to a resonant frequency of 43.71 THz and a resonant wavelength of 6.83 µm. The associated full width at half maximum (FWHM) is 1.93 cm^{-1}, ie. 5.79 THz. Taking $\varepsilon_r = 13.5$ for the VO2 in its dielectric phase at 6.83 µm [9], we obtain according to the model presented below, L' = $2.3845 \cdot 10^{-12}$ H and C = $1.24095 \cdot 10^{-17}$ F. With a gold resistivity of $\rho_{Au} = 22 \cdot 10^{-9}$ Ω·m and a gold electronic density of $n_{Au} = 5.9 \cdot 10^{28}$ m^{-3} [1], we get with the standard

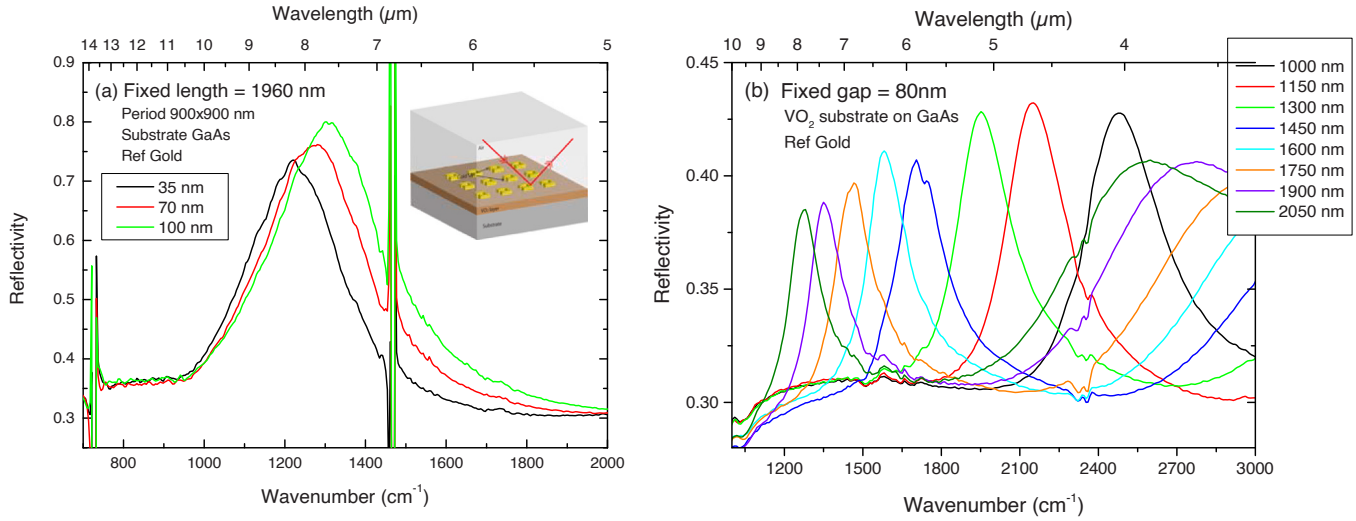

Fig. 4. (a) Experimental reflectivity measurements of SRR arrays with a varying gap (35 nm, 70 nm, 100 nm), a total length fixed at 1960 nm and a period fixed at 900 nm on a GaAs substrate. Inset: Schematic of the reflectivity measurement with an optical microscope and a FTIR spectrometer. (b) Experimental reflectivity measurements of SRR arrays with a varying total length from 1000 nm to 2050 nm, a gap fixed at 80 nm and a periodicity increasing proportionally to the total length. Substrate is a VO_2/GaAs bi-layer.

definition of the resistance $R = \rho\frac{\ell}{S} = \rho\frac{\ell}{wh}$ a value of R = 4.6386 Ω and the plasma pulsation is calculated to be $\omega_p = 1.37{\cdot}10^{16}$ rad·s^{-1}. The inductance equals L = $1.27{\cdot}10^{-13}$ H. We confirm that we have $L \gg L$. With the theoretical model, we thus estimate the resonant pulsation to be $\omega_r = 1.79{\cdot}10^{14}$ rad·s^{-1} and the corresponding resonant frequency to be f_r = 28.5 THz. The pulsation FWHM is $0.36{\cdot}10^{14}$ rad·s^{-1}, equivalent of a frequency FWHM of 5.81 THz. The comparison of the experimental and theoretical FWHM is in very good agreement. The resonance frequency based on the model is slightly shifted with the experimental value. This shift is due to the VO_2 permittivity taken from the literature, a value of $\varepsilon_r = 5.7$ (refractive index of 2.38) could cancel this shift.

Fig. 5 presents the experimental measure of the reflectivity versus temperature for a MM array of a fixed SRR geometry of 1.75 μm length and a gap of 80 nm on a 150 nm thick VO_2 film deposited on a GaAs substrate. The measurements have been performed below and above the VO_2 transition temperature using a regulated heating and cooling platform.

At low temperature, VO_2 behaves as a dielectric, the measured reflectivity presents a maximum, which corresponds to the LC cavity resonance. At high temperature, VO_2 has a metallic behavior, the measured reflectivity is high and flat, that is typical of the response of a continuous metallic plane and there is no phonon absorption band in this measurement range [2,27]. SRR are short-circuited and there is no more resonance. In the regime of intermediate temperature, shown in the zoom of Fig. 5.b, the global reflectivity increases according to the temperature whereas the SRR resonance maximum decreases through the VO_2 phase transition and the FWHM of the resonant peak gets wider. This resonance maximum is situated around 1450 cm^{-1} and shifts of 100 cm^{-1} along the phase transition on a temperature range of the order of 10°C, between 65°C and 72°C. Tunability is of the order of 7 %. During the phase transition, the optical width of the resonators changes, increasing the capacitance and the inductance of the SRR and thus reducing the resonance frequency. A shift towards low frequencies (red

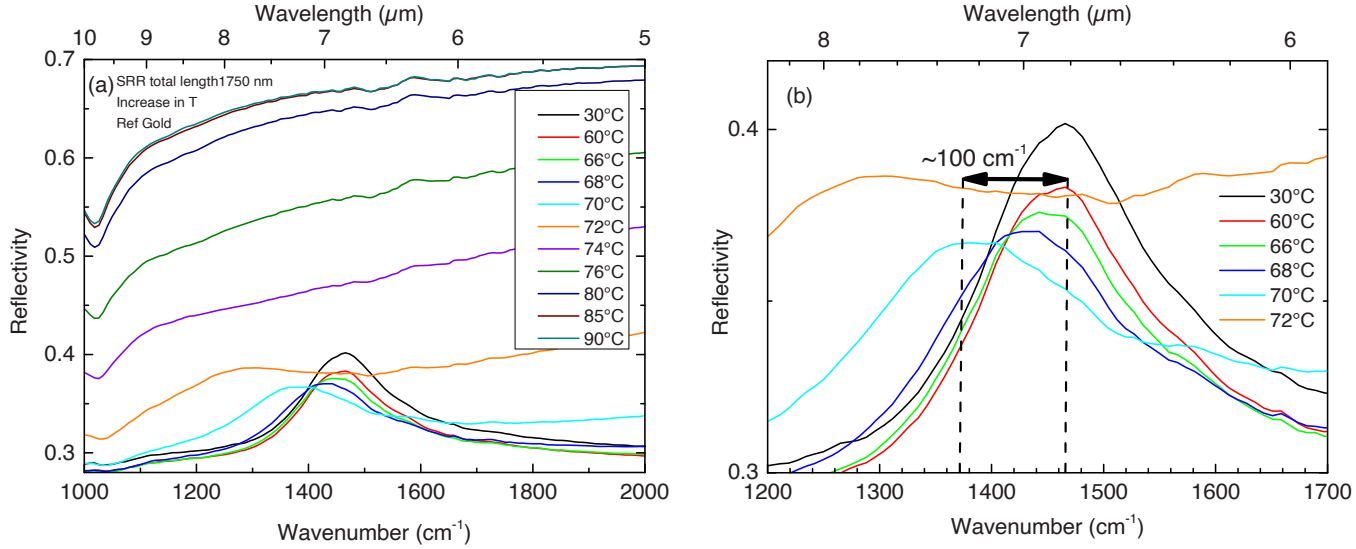

Fig. 5. (a) Experimental reflectivity measurement of a SRR array on a VO_2/GaAs bi-layer substrate for an increase in temperature. Geometry is fixed to 1750 nm for the total length and to 80 nm for the gap. (b) Zoom on the resonance in the middle of the phase change transition of VO_2. Tunability of 100 cm^{-1} is achieved between 60°C (red curve) and 70°C (light blue curve). Background line increases during the transition when VO_2 becomes metallic and makes the SRR resonance disappear.

shift) is obtained.

In conclusion, we showed in this study that the homogeneous and resonant response of SRR meta-surfaces arrays below the diffraction limit can be tuned in frequency in a static way and a dynamic way. Varying the geometric parameters adjusts the SRR resonance frequency, which is more sensitive to the gap variation than to the total length variation. Furthermore, we demonstrate that for a fixed geometry, it is possible to tune the resonance frequency using vanadium dioxide VO_2 phase change material. The deposition of a SRR array on a VO_2 layer grown by pulsed laser deposition on a GaAs substrate enabled an optical modulation of more than 100 cm^{-1} of the resonance peak during the VO_2 phase transition. Thus, associating meta-materials and phase change materials allows the choice and the tuning of the resonance frequency of the bi-layer. This result is very promising for the conception of monolithic, robust, compact, frequency tunable III-V based devices in the mid-infrared and whose optical properties only depend on the VO_2 layer temperature.

CRediT authorship contribution statement

Paul Goulain: Conceptualization, Investigation. **Laurent Boulley:** Conceptualization, Data curation, Formal analysis, Visualization, Writing – original draft, Writing – review & editing. **Adel Bousseksou:** Conceptualization, Data curation, Formal analysis, Funding acquisition, Investigation, Methodology, Project administration, Resources, Software, Supervision, Validation, Visualization, Writing – original draft, Writing – review & editing. **Raffaele colombelli:** Conceptualization, Funding acquisition, Investigation, Resources, Supervision, Visualization, Writing – original draft. **Thomas Maroutian:** Conceptualization, Resources, Supervision. **Pierre Laffaille:** Conceptualization, Investigation.

Declaration of Competing Interest

The authors declare that they have no known competing financial interests or personal relationships that could have appeared to influence the work reported in this paper.

Data availability

Data will be made available on request.

Acknowledgements

We acknowledge financial support from the French research agency ANR Grant ATLAS (ANR-14-CE26-0004-01) and the Agence Française pour la Promotion de l'Enseignement Supérieur, l'Accueil et la Mobilité Internationale (Project 38256QC). This work was partly supported by the French RENATECH network cleanroom facilities. The data that supports the findings of this study are available within the article. We also wish to thank J-M Manceau, P. Lecœur and G. Agnus for the useful scientific exchange.

References

[1] N.W. Ashcroft, N.D. Mermin, Solid State Physics. HRW international editions. Holt, Rinehart and Winston, 1976.
[2] A.S. Barker, H.W. Verleur, H.J. Guggenheim, Infrared optical properties of vanadium dioxide above and below the transition temperature, Phys. Rev. Lett. 17 (26) (1966) 1286–1289. URL: http://link.aps.org/doi/10.1103/PhysRevLett.17.1286.
[3] L. Boulley, T. Maroutian, P. Goulain, et al., Low temperature deposition of vanadium dioxide on III–V semiconductors and integration on mid-infrared quantum cascade lasers (January), AIP Adv. 13 (1) (2023) 015315, https://doi.org/10.1063/5.0111159.
[4] N.A. Butakov, I. Valmianski, T. Lewi, et al., Switchable plasmonic-dielectric resonators with metal-insulator transitions, ACS Photonics 5 (2) (2018) 371–377, https://doi.org/10.1021/acsphotonics.7b00334.
[5] W. Cai, V. Shalaev, Optical Metamaterials. Fundamentals and Applications, Springer Science, 2010, https://doi.org/10.1007/978-1-4419-1151-3.
[6] H.-T. Chen, W.J. Padilla, J.M.O. Zide, et al., Active terahertz metamaterial devices, URL: https://doi.org/10.1038/nature05343, Nature 444 (2006) 597–600, https://doi.org/10.1038/nature05343.
[7] H.-T. Chen, S. Palit, T. Tyler, et al., Hybrid metamaterials enable fast electrical modulation of freely propagating terahertz waves, URL: https://doi.org/10.1063/1.2978071, Appl. Phys. Lett. 93 (9) (2008) 091117, https://doi.org/10.1063/1.2978071.
[8] C. Cohen-Tannoudji, B. Diu, F. Laloë, Mécanique Quantique. Collection Enseignement des sciences, Hermann, 1998.
[9] M.J. Dicken, K. Aydin, I.M. Pryce, et al., Frequency tunable near-infrared metamaterials based on VO_2 phase transition, URL: https://www.osapublishing.org/oe/abstract.cfm?uri=oe-17-20-18330, Opt. Express 17 (20) (2009) 18330, https://doi.org/10.1364/OE.17.018330.
[10] T. Driscoll, S. Palit, M.M. Qazilbash, et al., Dynamic tuning of an infrared hybrid-metamaterial resonance using vanadium dioxide, URL: https://doi.org/10.1063/1.2956675, Appl. Phys. Lett. 93 (2) (2008) 024101, https://doi.org/10.1063/1.2956675.
[11] F. Dumas-Bouchiat, C. Champeaux, A. Catherinot, et al., RF-microwave switches based on reversible semiconductor-metal transition of VO_2 thin films synthesized by pulsed-laser deposition, URL: https://doi.org/10.1063/1.2815927, Appl. Phys. Lett. 91 (22) (2007) 223505, https://doi.org/10.1063/1.2815927.
[12] K. Fan, W.J. Padilla, Dynamic electromagnetic metamaterials, URL: https://doi.org/10.1016/j.mattod.2014.07.010, Mater. Today 18 (1) (2015) 39–50, https://doi.org/10.1016/j.mattod.2014.07.010.
[13] P. Hosseini, C.D. Wright, H. Bhaskaran, An optoelectronic framework enabled by low-dimensional phase-change films, Nature 511 (2014) 206–211, https://doi.org/10.1038/nature13487.
[14] A. Ishikawa, T. Tanaka, S. Kawata, Negative magnetic permeability in the visible light region, Phys. Rev. Lett. 95 (23) (2005) 5–8, https://doi.org/10.1103/PhysRevLett.95.237401.
[15] J.D. Jackson, Classical Electrodynamics, John Wiley & Sons, 1999.
[16] M. Kafesaki, E.N. Economou, C.M. Soukoulis, et al., Saturation of the MAgnetic Response of Split-ring Resonators at Optical Frequencies, Phys. Rev. Lett. 95 (22) (2005), https://doi.org/10.1103/physrevlett.95.223902.
[17] M.W. Klein, C. Enkrich, M. Wegener, et al., Single-slit split-ring resonators at optical frequencies: limits of size scaling, Opt. Lett. 31 (9) (2006) 1259, https://doi.org/10.1364/ol.31.001259.
[18] M. Liu, H.Y. Hwang, H. Tao, et al., Terahertz-field-induced insulator-to-metal transition in vanadium dioxide metamaterial, URL: https://doi.org/10.1038/nature11231, Nature 487 (7407) (2012) 345–348, https://doi.org/10.1038/nature11231.
[19] Y. Lu, M. Stegmaier, P. Nukala, et al., Mixed-mode operation of hybrid phase-change nanophotonic circuits, Nano Lett. 17 (1) (2017) 150–155, https://doi.org/10.1021/acs.nanolett.6b03688.
[20] M.T. Nouman, J.H. Hwang, M. Faiyaz, et al., Vanadium dioxide based frequency tunable metasurface filters for realizing reconfigurable terahertz optical phase and polarization control, URL: http://www.opticsexpress.org/abstract.cfm?URI=oe-26-10-12922, Opt. Express 26 (10) (2018) 12922–12929, https://doi.org/10.1364/OE.26.012922.
[21] J.M. Manceau, N.H. Shen, M. Kafesaki, et al., Dynamic response of metamaterials in the terahertz regime: blueshift tunability and broadband phase modulation, Appl. Phys. Lett. 96 (2) (2010) 2008–2011, https://doi.org/10.1063/1.3292208.
[22] S. O'Brien, J.B. Pendry, Magnetic activity at infrared frequencies in structured metallic photonic crystals, J. Phys. Condens. Matter 14 (25) (2002) 6383–6394, https://doi.org/10.1088/0953-8984/14/25/307.
[23] W.J. Padilla, A.J. Taylor, C. Highstrete, Dynamical electric and magnetic metamaterial response at terahertz frequencies. Conference on Lasers and Electro-Optics and 2006 Quantum Electronics and Laser Science Conference,CLEO/QELS 2006, 107401(March):1–4, 2006. doi:10.1109/CLEO.2006.4627768.
[24] J.B. Pendry, A.J. Holden, D.J. Robbins, et al., Magnetism from conductors and enhanced nonlinear phenomena, arXiv:1403.6488, IEEE Trans. Microw. Theory Tech. 47 (11) (1999) 2075–2084, https://doi.org/10.1109/22.798002.
[25] J.B. Pendry, Negative refraction makes a perfect lens, URL: https://link.aps.org/doi/10.1103/PhysRevLett.85.3966, Phys. Rev. Lett. 85 (2000) 3966–3969, https://doi.org/10.1103/PhysRevLett.85.3966.
[26] J.B. Pendry, D. Schurig, D.R. Smith, Controlling electromagnetic fields, URL: https://science.sciencemag.org/content/312/5781/1780, Science 312 (5781) (2006) 1780–1782, https://doi.org/10.1126/science.1125907.
[27] W.W. Peng, G. Niu, R. Tétot, et al., Insulator-metal transition of VO_2 ultrathin films on silicon: evidence for an electronic origin by infrared spectroscopy, J. Phys. Condens. Matter 25 (44) (2013), https://doi.org/10.1088/0953-8984/25/44/445402.
[28] W.H.P. Pernice, H. Bhaskaran, Photonic non-volatile memories using phase change materials (URL), Appl. Phys. Lett. 101 (2012) 171101, https://doi.org/10.1063/1.4758996.
[29] C. Ríos, M. Stegmaier, P. Hosseini, et al., Integrated all-photonic non-volatile multi-level memory, Nat. Photonics 9 (2015) 725–732, https://doi.org/10.1038/NPHOTON.2015.182.
[30] M. Rudé, J. Pello, R.E. Simpson, et al., Optical switching at 1.55μm in silicon racetrack resonators using phase change materials, Appl. Phys. Lett. 103 (2013) 141119, https://doi.org/10.1063/1.4824714.
[31] A.E. Siegman, Lasers, University Science Books, 1986.

[32] A.M. Shaltout, N. Kinsey, J. Kim, et al., Development of optical metasurfaces: emerging concepts and new materials, arXiv:arXiv:1112.2766v1, Proc. IEEE 104 (12) (2016) 2270–2287, https://doi.org/10.1109/JPROC.2016.2590882.

[33] N.H. Shen, M. Massaouti, M. Gokkavas, et al., Optically implemented broadband blueshift switch in the terahertz regime, URL: https://link.aps.org/doi/10.1103/PhysRevLett.106.037403, Phys. Rev. Lett. 106 (2011) 037403, https://doi.org/10.1103/PhysRevLett.106.037403.

[34] D.R. Smith, W.J. Padilla, D.C. Vier, et al., Composite medium with simultaneously negative permeability and permittivity, URL: https://link.aps.org/doi/10.1103/PhysRevLett.84.4184, Phys. Rev. Lett. 84 (2000) 4184–4187, https://doi.org/10.1103/PhysRevLett.84.4184.

[35] D.R. Smith, J.B. Pendry, M.C.K. Wiltshire, Metamaterials and negative refractive index, URL: http://science.sciencemag.org/content/305/5685/788, arXiv:http://science.sciencemag.org/content/305/5685/788.full.pdf, Science 305 (5685) (2004) 788–792, https://doi.org/10.1126/science.1096796.

[36] V.G. Veselago, The electrodynamics of substances with simultaneously negative values of ε and μ, Sov. Phys. Uspekhi 10 (4) (1968) 509. URL: http://stacks.iop.org/0038-5670/10/i=4/a=R04.

[37] Z. Yang, C. Ko, S. Ramanathan, Oxide electronics utilizing ultrafast metal-insulator transitions, Annu. Rev. Mater. Res. 41 (1) (2011) 337–367, https://doi.org/10.1146/annurev-matsci-062910-100347.

[38] C. Zhang, G. Zhou, J. Wu, et al., Active control of terahertz waves using vanadium-dioxide-embedded metamaterials, URL: https://link.aps.org/doi/10.1103/PhysRevApplied.11.054016, Phys. Rev. Appl. 11 (5) (2019) 054016, https://doi.org/10.1103/PhysRevApplied.11.054016.

[39] H. Zhang, L. Zhou, L. Lu, et al., Miniature multilevel optical memristive switch using phase change material, ACS Photonics 6 (9) (2019) 2205–2212, https://doi.org/10.1021/acsphotonics.9b00819.

[40] N.I. Zheludev, Y.S. Kivshar, From metamaterials to metadevices, URL: https://doi.org/10.1038/nmat3431, arXiv:1232009, Nat. Mater. 11 (11) (2012) 917–924, https://doi.org/10.1038/nmat3431.

[41] H. Zhu, Y. Lu, L. Cai, Wavelength-shift-free racetrack resonator hybrided with phase change material for photonic in-memory computing (URL:), Opt. Express 31 (12) (2023), https://doi.org/10.1364/OE.489525.